AD-768 379

BALLISTIC SKIP GUIDANCE FOR ATMOSPHERIC RE-ENTRY

Melvin L. Nagel

Air Force Institute of Technology
Wright-Patterson Air Force Base, Ohio

June 1973

DISTRIBUTED BY:

NTIS
National Technical Information Service
U. S. DEPARTMENT OF COMMERCE
5285 Port Royal Road, Springfield Va. 22151

Unclassified
Security Classification

DOCUMENT CONTROL DATA - R & D

(Security classification of title, body of abstract and indexing annotation must be entered when the overall report is classified)

ORIGINATING ACTIVITY (Corporate author) Air Force Institute of Technology (AFIT-SE) Wright-Patterson AFB, Ohio 45433	2a. REPORT SECURITY CLASSIFICATION Unclassified 2b. GROUP

3. REPORT TITLE

BALLISTIC SKIP GUIDANCE FOR ATMOSPHERIC RE-ENTRY

4. DESCRIPTIVE NOTES (Type of report and inclusive dates)

AFIT Thesis

5. AUTHOR(S) (First name, middle initial, last name)

Melvin L. Nagel
1Lt USAF

6. REPORT DATE June 1973	7a. TOTAL NO. OF PAGES 48	7b. NO. OF REFS 5
8a. CONTRACT OR GRANT NO b. PROJECT NO. c. d.	9a. ORIGINATOR'S REPORT NUMBER(S) GGC/EE/73-10 9b. OTHER REPORT NO(S) (Any other number) that may be assigned this report)	

10. DISTRIBUTION STATEMENT

Approved for public release; distribution unlimited.

11. SUPPLEMENTARY NOTES Approved for public release; IAW AFR 190-17 JERRY C. HIX, Captain, USAF Director of Information	12. SPONSORING MILITARY ACTIVITY Air Force Flight Dynamics Laboratory Wright-Patterson AFB, Ohio 45433

13. ABSTRACT

The feasibility of a re-entry guidance scheme that utilizes ballistic flight to attain a variable surface range is investigated. The equations of motion are derived, and the re-entry trajectory is divided into four phases: pull up, skipout, ballistic, and terminal. The pull up, skipout, and terminal phases are within the atmosphere, while the ballistic phase is outside the atmosphere. The conjugate gradient optimization method is used in the skipout phase to determine the re-entry vehicle control needed to achieve the desired initial ballistic phase conditions. The cost function uses the errors between the actual trajectory and a reference trajectory which is obtained by projecting a ballistic path into the atmosphere. The equations for the reference trajectory are presented. Ballistic theory is discussed and a parametric selection technique is presented as a means of determining the ballistic parameters needed for a specific range. An optimal control solution is found for one set of ballistic initial conditions.

Reproduced by
NATIONAL TECHNICAL
INFORMATION SERVICE
U S Department of Commerce
Springfield VA 22151

DD FORM 1 NOV 65 1473

Unclassified
Security Classification

10

14. KEY WORDS	LINK A ROLE	LINK A WT	LINK B ROLE	LINK B WT	LINK C ROLE	LINK C WT
Re-entry Guidance						
Ballistic Skip Re-entry						
Parameterization of Free Flight Range Angle						
Conjugate Gradient Optimization						
Optimal Control Tracking						

AD 768379

BALLISTIC SKIP GUIDANCE

FOR ATMOSPHERIC RE-ENTRY

THESIS

GGC/EE/73-10

Melvin L. Nagel
1Lt USAF

Approved for public release;
distribution unlimited.

GGC/EE/73-10

BALLISTIC SKIP GUIDANCE FOR ATMOSPHERIC RE-ENTRY

THESIS

Presented to the Faculty of the School of Engineering of

the Air Force Institute of Technology

Air University

in Partial Fulfillment of the

Requirements for the Degree of

Master of Science

by

Melvin L. Nagel, B.S.E.E.
1Lt USAF

Graduate Guidance and Control

Electrical Engineering

June 1973

Approved for public release; distribution unlimited.

1C

Preface

In the midst of the successful Apollo moon missions, I became interested in astrodynamics. Fortunately, after being sent to AFIT, I had the opportunity to take the sequence of astronautical courses. Soon after taking an astrodynamical guidance course, this thesis topic caught my eye. Now, after trying my own hand at spacecraft guidance schemes, even though only in two-dimensions, I can really appreciate the complexities that must be involved in a moon mission.

I wish to express appreciation to my advisor, Major James Funk, Department of Electrical Engineering, AFIT, for his advice and help in the completion of this thesis. In addition, the aid of Captain David South, AFFDL, who provided me with many reference papers, is gratefully acknowledged. Special thanks go to two of my fellow students, First Lieutenants Phil Hollister and Dean Navin, for the many hours of companionship, humor, and advice during the thesis quarters.

Melvin L. Nagel

Contents

	Page
Preface	ii
List of Figures	v
List of Tables	vi
List of Symbols	vii
Abstract	x
I. Introduction	1
Background	1
Purpose and Scope	2
Method of Analysis	2
Overview	4
II. Mathematical Model	5
Assumptions	5
Aerodynamic Model	5
Equations of Motion	6
Heating and Deceleration Equations	7
III. Problem Formulation	8
Phase Definition	8
Ballistic Theory	8
Range Allocation	10
Reference Trajectory	16
Conjugate Gradient Equations	20
Computer Methods	23
IV. Results	25
V. Conclusions	33

Contents

	Page
Bibliography	35
Appendix A: Derivation of Equations of Motion	36
Appendix B: Conjugate Gradient Theory	44
Appendix C: Plot of Lift Coefficient versus Angle of Attack	47
Vita	48

List of Figures

Figure		Page
1	Trajectory Phase Definition	9
2	Q and δ vs. Δ	13
3	Range Angle vs. Δ	14
4	Ballistic Phase Range Division	15
5	A Ballistic Trajectory	17
6	Actual and Reference Trajectory During Skipout	19
7	Optimal Altitude Trajectory	28
8	Optimal Q Trajectory	29
9	Optimal Flight Path Angle Trajectory	30
10	Optimal Control Trajectory	31
11	Geometry of the Problem	37
12	Lift Coefficient vs. Angle of Attack	47

List of Tables

Table		Page
I	Pull up Phase End Conditions	26
II	Cost Function Weighting Values	26
III	Conjugate Gradient Terminal Errors	32
IV	Total Surface Range.	32

List of Symbols

A	Error weighting matrix
a	Total acceleration
B	Control movement weighting scalar
C	Coordinate transformation matrix
C_D	Coefficient of drag
C_L	Coefficient of lift
D	Drag
E	Earth centered coordinate frame
E*	Orbital specific mechanical energy
$\bar{e}$	Error vector
e*	Orbital eccentricity
F	Penalty weighting matrix
G	Gradient
g	Gravity
H	Hamiltonian
h	Altitude
h*	Orbital specific angular momentum
J	Conjugate gradient cost function
L	Lift
M	Vehicle centered, vertically-oriented, coordinate frame
N	Vehicle centered, velocity-oriented, coordinate frame
p*	Orbital semi-latus rectum
Q	Energy parameter equal to the squared ratio of actual velocity to local circular velocity
q	Total nose heat
R	Radius

List of Symbols

s	Surface range
s'	Step magnitude along direction of alpha search
t	Clock time
V	Total velocity
$\bar{x}$	State vector
$\frac{S}{m}$	The inverse of wing loading
α	Control (or angle of attack)
α'	Distance in alpha search
β	Atmospheric constant
β'	Alpha search correction factor
Δ	Stepping variable
δ	Flight path (depression) angle
ζ	Damping ratio
$\bar{\lambda}$	Adjoint vector
μ	Earth gravitational constant
ν	Angle from periapsis
ρ	Atmospheric density
σ	Total surface range
ψ	Ballistic phase surface range
ω	Angular rotation rate
ω_n	Undamped natural frequency

Subscripts

b	The reference trajectory
e	Earth
f	Final value

List of Symbols

h	Altitude, a state
o	Initial value
Q	The energy parameter, a state
so	Skipout point
δ	Flight path angle, a state

Abstract

The feasibility of a re-entry guidance scheme that utilizes ballistic flight to attain a variable surface range is investigated. The equations of motion are derived, and the re-entry trajectory is divided into four phases: pull up, skipout, ballistic, and terminal. The pull up, skipout, and terminal phases are inside the atmosphere, while the ballistic phase is outside the atmosphere. The conjugate gradient optimization method is used in the skipout phase to determine the re-entry vehicle control needed to achieve the desired initial ballistic phase conditions. The cost function uses the errors between the actual trajectory and a reference trajectory which is obtained by projecting a ballistic path into the atmosphere. The equations for the reference trajectory are presented. Ballistic theory is discussed and a parametric selection technique is developed as a means of determining the ballistic parameters needed for a specific range. An optimal control solution is found for one set of ballistic initial conditions.

I. Introduction

Background

Consider a spacecraft orbiting the moon, prior to a return flight to Earth. The time of departure from lunar orbit is dependent upon many variables, one of which is the Earth's rotation. That is, the location of the landing site moves with the Earth. The spacecraft must enter the atmosphere within a certain time period so that the landing site will be within range of its guidance capabilities. In the case of the recent Apollo missions, the maximum attainable surface range was approximately 2200 nautical miles (nm) (Ref 1). Alternate landing sites were available for the Apollo splashdowns, but every alternate site requires the use of additional recovery ships and other resources.

To eliminate the need for excessive backup landing areas, it is desirable to have a guidance scheme that will allow a re-entry vehicle (RV) more flexibility in surface range. Ideally, a spacecraft returning from the moon would be able to land at one fixed location, independent of the distance involved, including circumnavigation of the globe.

One method of attaining more surface range is by including a segment of ballistic flight in the re-entry trajectory. If the spacecraft is made to skipout of the atmosphere after initial entry, it would then be on a ballistic trajectory. Assuming the craft re-enters the atmosphere due to the Earth's gravitational influence, the surface distance traveled during ballistic flight would depend only upon the state of the vehicle at atmospheric exit (skipout conditions). The skipout conditions, in turn, would be a function of the total range desired. (When the term range is used alone, it will mean surface range).

Purpose and Scope

The purpose of this thesis is to investigate the feasibility of a re-entry guidance scheme that will utilize ballistic flight to achieve a variable surface range. The surface range refers to the total distance between the initial point of re-entry and the target point above the landing site.

The main emphasis of this study is placed upon 1) finding the skipout conditions for a desired ballistic trajectory, and 2) optimally driving the states of the RV to those skipout conditions. The control necessary to obtain the correct states is found by an optimization scheme.

The only type of re-entry considered directly in this study is one resulting from a lunar return flight, but extensions to other types could be made. Also, the g forces and the vehicle nose heating are not directly constrained.

Method of Analysis

The problem was attacked by dividing the trajectory into four distinct phases. The theory of ballistic flight was then considered in order to establish the necessary skipout conditions. It was decided that the normal method of calculating ballistic range (see equation (10)) would not suffice for the problem at hand, because the range was dependent upon two arbitrary variables. Consequently, a linear stepping technique was devised which would allow ballistic range, and hence the skipout conditions, to be an indirect function of only a stepping variable. Then, to simplify the analysis, the terminal phase was arbitrarily assigned a fixed value of range. This was done by assuming that a terminal phase guidance scheme could land the RV for a realistic range of state conditions occurring after ballistic flight.

Emphasis was then placed upon finding a method (guidance scheme) to attain the various skipout conditions. Several unsuccessful methods were initially tried. The first method was an attempt to derive a control law from the derivative of Q. Equation (7) was solved for the angle of attack and dQ/ds was defined as the slope of a straight line between the actual Q and the desired Q at skipout. This control law failed because it could not control the initial part of the flight, due to the amount of energy involved.

The second idea was to hold the derivative of the flight path angle at zero when the RV, during its upward flight, acquired the needed skipout angle. The idea was only partly successful because once the angle began to stray from the desired value, the errors could not be corrected. In an effort to make this second idea self-corrective, it was converted into a second order approximation by taking the second derivative of δ with respect to range. The resulting coefficient of $d\delta/ds$ was set equal to $2\zeta\omega_n$ and a control law was found by solving for the angle of attack (which was contained in the coefficient). The control law operated as a bang-bang controller in an attempt to function properly. Since a violent control is undesirable, this method was put aside.

The conjugate gradient optimization technique was finally chosen as a suitable means of finding a control that would drive the RV to the proper conditions. The conjugate gradient cost function for this problem is based upon the differences between the actual states of a re-entry vehicle and the states of an imaginary ballistic vehicle which is traveling on a ballistic path extended into the atmosphere. For a guidance scheme to function properly, the actual trajectory should converge to the projected path before ballistic flight begins.

Overview

The mathematical models are set up in Chapter II. The items presented are the simplifying assumptions, the atmospheric model, the vehicle lift and drag equations, a summary of the equations of motion (or states) and the vehicle heating and deceleration equations.

Chapter III then goes into the problem formulation. A typical reentry trajectory is divided into phases and a method of range allocation for the ballistic phase is developed. Included in the chapter is discussion of some ballistic equations, development of a reference trajectory, derivation of the equations needed in the conjugate gradient method, and discussion of the computer requirements.

Chapter IV then covers the results of this study, while Chapter V contains the conclusions.

There are three appendices to this report. The equations of motion are derived in Appendix A and the conjugate gradient theory is given in Appendix B. Appendix C shows a plot of angle of attack versus the lift coefficient.

II. Mathematical Model

Assumptions

The assumptions listed below were made in order to reduce the complexity of the problem while retaining the most important characteristics.

1. All motion is two-dimensional.

2. The Earth is non-rotating and is spherical in shape.

3. The only bodies considered are the Earth and the re-entry vehicle.

4. The Earth's atmosphere above an altitude of 400,000 feet is neglected.

5. Below 400,000 feet in altitude, the atmospheric density is considered a function of altitude only, as expressed by the model

$$\rho = \rho_o \, e^{-\beta h} \tag{1}$$

where ρ_o is sea level density

$$\rho_o = 0.0026703 \text{ slugs/ft}^3$$

and β is an atmospheric constant

$$\beta = 0.0000425211877 \text{ ft}^{-1}$$

Aerodynamic Model

In addition, it is assumed that control of the re-entry vehicle will be accomplished by directly changing the angle of attack of the vehicle. The resulting lift and drag specific forces can be represented as

$$L = \frac{1}{2} \frac{S}{m} \rho \, V^2 \, C_L \tag{2}$$

$$D = \frac{1}{2}\frac{S}{m}\rho V^2 C_D \tag{3}$$

The inverse wing loading, $\frac{S}{m}$, is 1.18070 ft^2/slug. The lift and drag coefficients. for a hypersonic lifting body (Ref 2), are represented as Newtonian-Flat-Plate drag polars and are as shown.

$$C_L = 1.82 \sin\alpha \cos\alpha \, |\sin\alpha| \tag{4}$$

$$C_D = 0.042 + 1.46 \, |\sin^3\alpha| \tag{5}$$

For this vehicle model then, $(L/D)_{max} = 2$

The assumptions and models are used in the derivation of the equations of motion.

Equations of Motion

The equations of motion were written relative to an inertial, Earth centered, coordinate system. The equations (see Appendix A for the derivation) are represented as derivatives with respect to surface range, s, and they are listed here for continuity.

$$\frac{dx_1}{ds} = \frac{dh}{ds} = -\frac{R}{R_e}\tan\delta \tag{6}$$

$$\frac{dx_2}{ds} = \frac{dQ}{ds} = \left(\tan\delta\,(2-Q) - R\rho\,\frac{S}{m}\sec\delta\, Q\, C_D\right)\frac{1}{R_e} \tag{7}$$

$$\frac{dx_3}{ds} = \frac{d\delta}{ds} = \left(\frac{1}{Q} - 1 - R\rho\,\frac{S}{2m}\sec\delta\, C_L\right)\frac{1}{R_e} \tag{8}$$

where h is the altitude above sea level, Q is an energy parameter (defined in Chapter III), δ is the flight depression angle, and $R = R_e + h$.

$$R_e = 20925738 \text{ ft}$$

is the radius of the Earth, taken from Bate (Ref 3).

Heating and Deceleration Equations

Although vehicle nose heating and deceleration forces were not directly constrained, they were observed to insure that the magnitudes were reasonable.

The total heat was obtained by integration of the heat rate

$$\frac{dq}{ds} = C_{heat}\, \rho^{\frac{1}{2}}\, V^2 \sec\delta\, \frac{R}{R_e} \tag{8a}$$

where $C_{heat} = 2 \times 10^{-8}$ BTU·sec^2/ft$^{\frac{7}{2}}$·slugs$^{\frac{1}{2}}$

is the heating coefficient.

Deceleration was computed from the time derivative of velocity, i.e.,

$$\frac{dv}{dt} = \frac{\mu}{R^2} \sin\delta - D \tag{62}$$

where $\mu = 1.407654 \times 10^{16}$ ft^3/sec^2 (from Ref 3) is the Earth's gravitational constant.

III. Problem Formulation

Phase Definition

To simplify the problem analysis, the re-entry trajectory is separated into four distinct phases which are shown in Fig. 1 and are defined below. A flat Earth representation is used in the figure for ease of illustration.

1. Pull up Phase - - That part of the trajectory from initial re-entry at 400,000 feet to the point where the flight path angle, δ, initially changes sign (from positive to negative).

2. Skipout Phase - - That part of the trajectory from the point where δ changes sign, as mentioned above, to the point where the RV leaves the atmosphere. The guidance scheme is used in this phase.

3. Ballistic Phase - - That part of the trajectory occurring above 400,000 feet, where ballistic theory governs flight. The state values at the beginning of this phase are referred to as the skipout (so), or skip, conditions.

4. Terminal Phase - - That part of the trajectory following ballistic flight. It begins at 400,000 feet and ends with a landing on Earth.

Ballistic Theory

Ballistic, or free flight theory is not new. Equations describing ballistic motion indicate that ranges up to halfway around the globe (approximately 10,800 nm) are possible for values of $Q_{so} \leq 1$. For $Q_{so} > 1$, greater ranges are possible (see Ref 3).

Q is a non-dimensional parameter defined as

$$Q = \frac{V^2 R}{\mu} \tag{9}$$

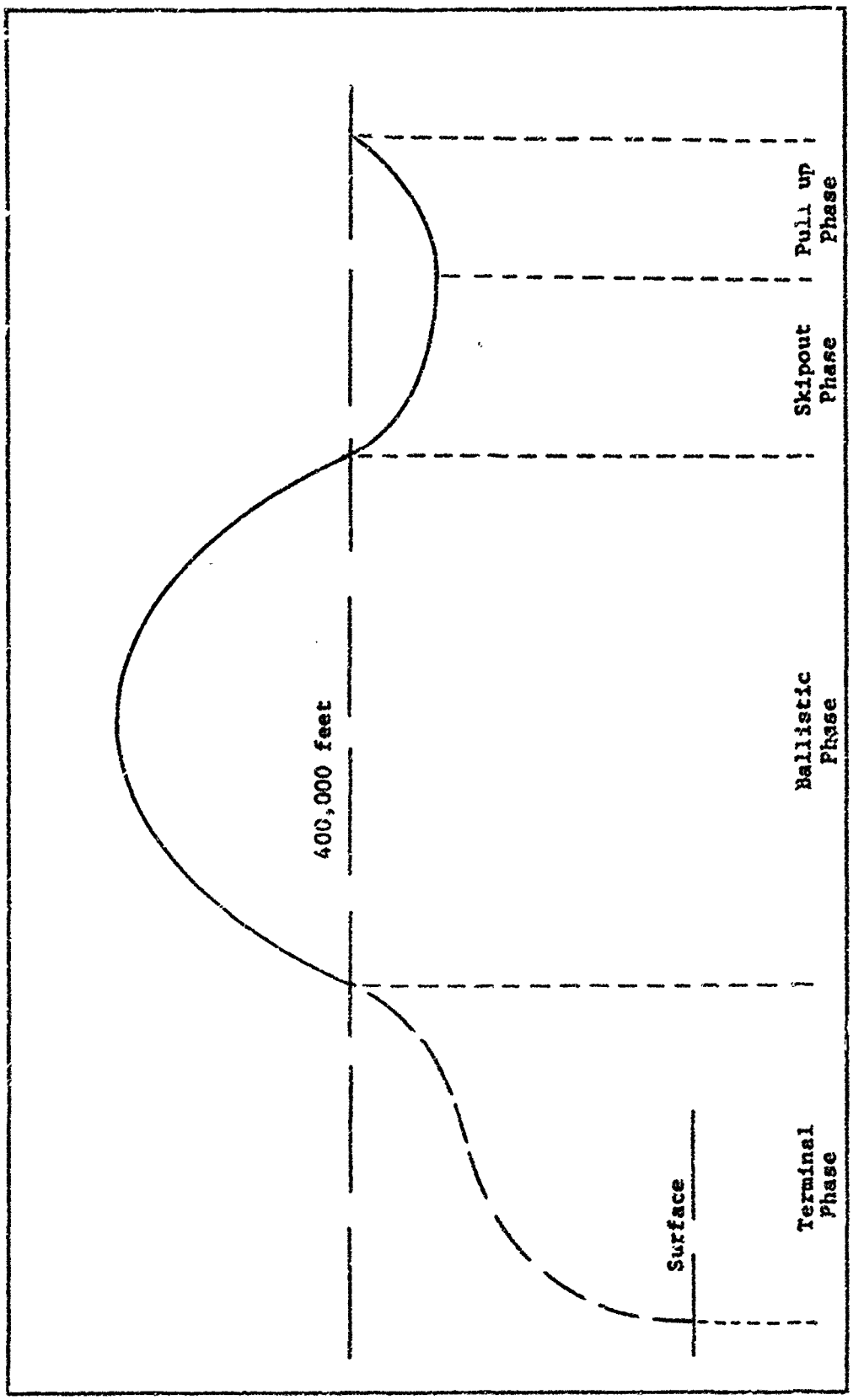

Fig. 1. Trajectory Phase Definition

The values of Q_{so} and δ_{so} (skipout conditions) are used to predict the range attainable for a particular ballistic flight. Since many different values of range are possible for the many different combinations of Q_{so} and δ_{so}, the ballistic phase is where most of the range adjustments will be made.

An important feature of a ballistic trajectory is that it is symmetric (see Fig. 5). If Q and δ are known at the beginning of free flight, the reflected skipout conditions will exist at the end of free flight, provided the initial and final radii are equal. The vehicle in this study will leave and enter the atmosphere at the same altitude, so the states of the RV at the end of the skipout phase must be a reflection of the states at the beginning of the terminal phase.

Range Allocation

It was mentioned in the previous section that variation of the skipout conditions causes a range variation between the beginning and end points of ballistic flight. The free flight range angle, ψ, is normally calculated from

$$\psi = \arccos \left[\frac{1 - Q_{so} \cos^2 \delta_{so}}{\sqrt{1 + Q_{so}(Q_{so} - 2)\cos^2 \delta_{so}}} \right] \tag{10}$$

However, equation (10) depends upon two variables, Q_{so} and δ_{so}, both of which may be arbitrarily varied. Also, there is no unique combination of Q_{so} and δ_{so} for many choices of desired range angle.

Finding a unique solution is possible by, in effect, reducing the number of variables to one. This is accomplished by using a linear stepping technique, which was arbitrarily selected in the form shown below.

$$Q_{so} = Q_1 + (Q_2 - Q_1)\Delta \tag{11}$$

$$\delta_{so} = \delta_1 + (\delta_2 - \delta_1)\Delta \tag{12}$$

or an alternate to equation (12) could be written

$$\delta_{so} = \delta_2 - (\delta_2 - \delta_1)\Delta \tag{13}$$

where Δ is a parametric stepping variable that ranges from 0 to 1, and the numerical subscripts refer to the upper and lower bounds on Q_{so} and δ_{so}.

After selecting upper and lower bounds, the values of Q_{so} and δ_{so} necessary for a desired range angle are dependent only upon the value of Δ.

Equations (11), (12), and (13) are plotted in Fig. 2 for an arbitrary choice of values, i.e.

$$Q_1 = .9 \leq Q_{so} \leq 1.4 = Q_2$$

$$\delta_1 = 2^\circ \leq \delta_{so} \leq 7^\circ = \delta_2$$

Notice that only the magnitude of the flight depression angle is needed for this discussion. In Fig. 2, the symbol 'x' corresponds to equation (12), the symbol '0' corresponds to equation (13), and the small symbol 'Δ' corresponds to equation (11).

Using the stepping variable to find values of Q_{so} and δ_{so}, from equations (11) and (12) or (13), corresponding values of range angle are

generated from equation (10). The range angles, as a function of the stepping variable, are plotted in Fig. 3. In that figure, the symbol 'x' is associated with the 'x' in Fig. 2, and similiarly for the other axis. Referring to Fig. 3 and choosing either 'x' (equation (12)) or 'O' (equation (13)) for a particular range depends upon the range desired and the slope of the range curves.

For short ranges, equation (12) would be used to find δ_{so}, and for long ranges, equation (13) would be used. For any intermediate range, the range curve with the least slope would dictate which equation would provide the least sensitivity to terminal errors in δ_{so}. Therefore, a logical division of ranges is shown in Fig. 4, which is merely Fig. 3 with certain segments deleted. Given a desired range, Fig. 4 indicates which equation is needed for calculation of the flight path angle since the symbol 'x' implies use of equation (11) and the symbol 'O' implies use of equation (12).

By examining Fig. 4, and the computer printout of data (not shown), one can find that the ballistic range for the current choices of Q_1, Q_2, δ_1, and δ_2 is 34.5° (2070 nm) to 346° (20,760 nm).

The total range angle, σ, is dependent upon how much distance the remaining three phases can add. For simplicity, it would be desirable for one or more of the other phases to have a fixed value of attainable range.

The terminal phase is singled out for this purpose, because the only item of interest here is how much range can the terminal guidance scheme cover. For the purpose of this study, it is assumed that a guidance scheme exists which will provide a nominal range of 1000 nm (chosen arbitrarily). The assumed guidance must be able to use, as initial conditions,

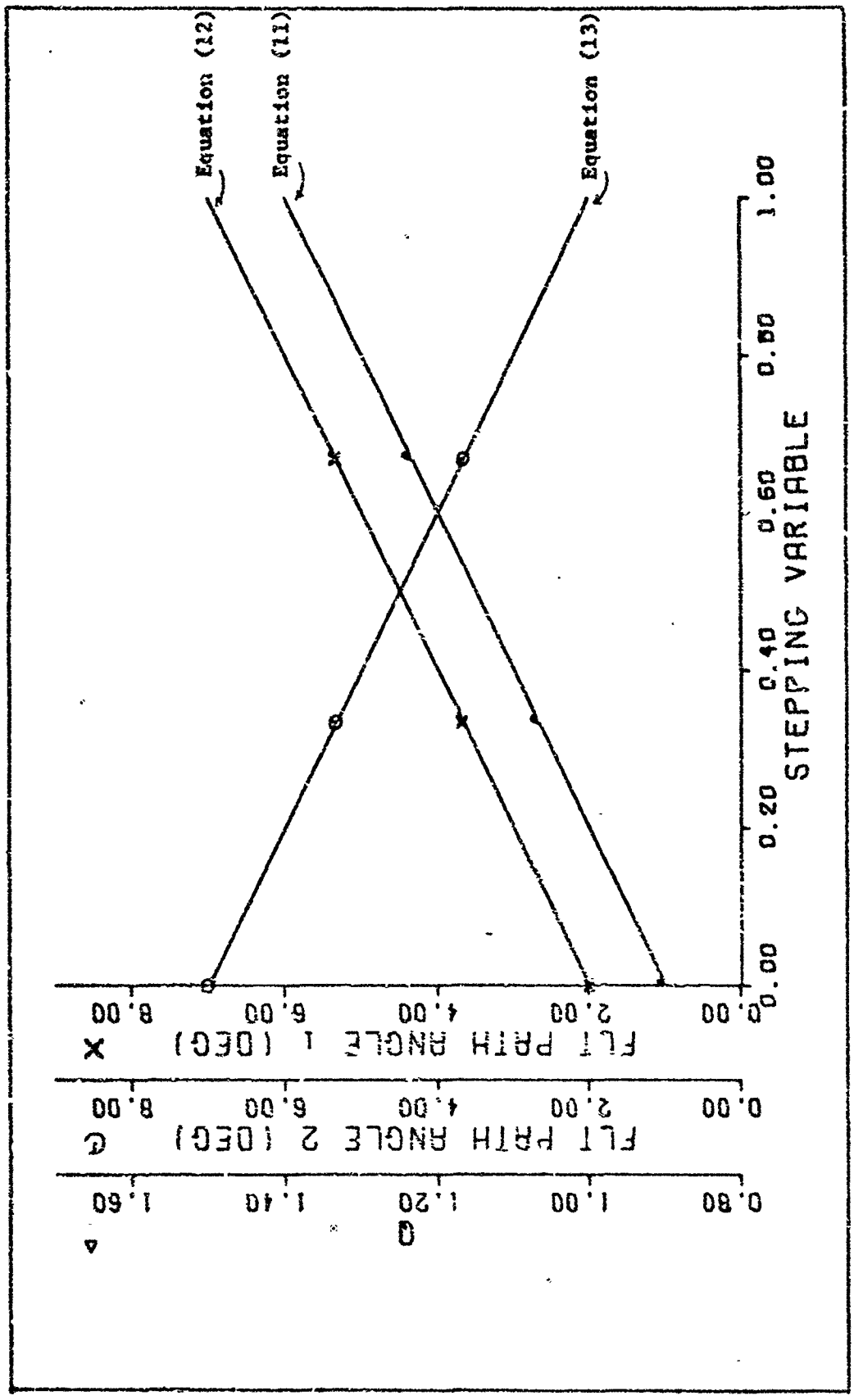

Fig. 2. Q and δ vs. Δ

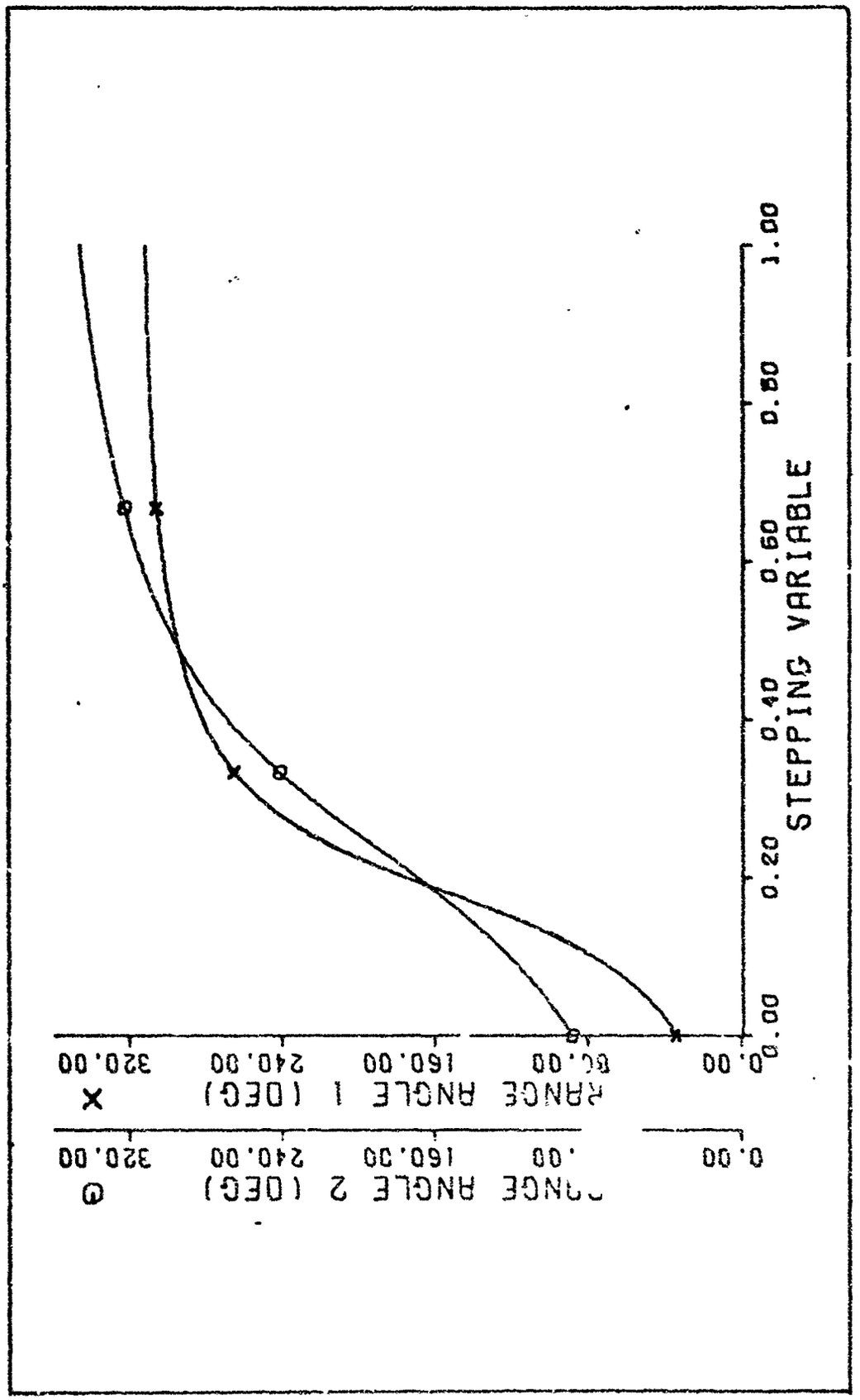

Fig. 3. Range Angle vs. Δ

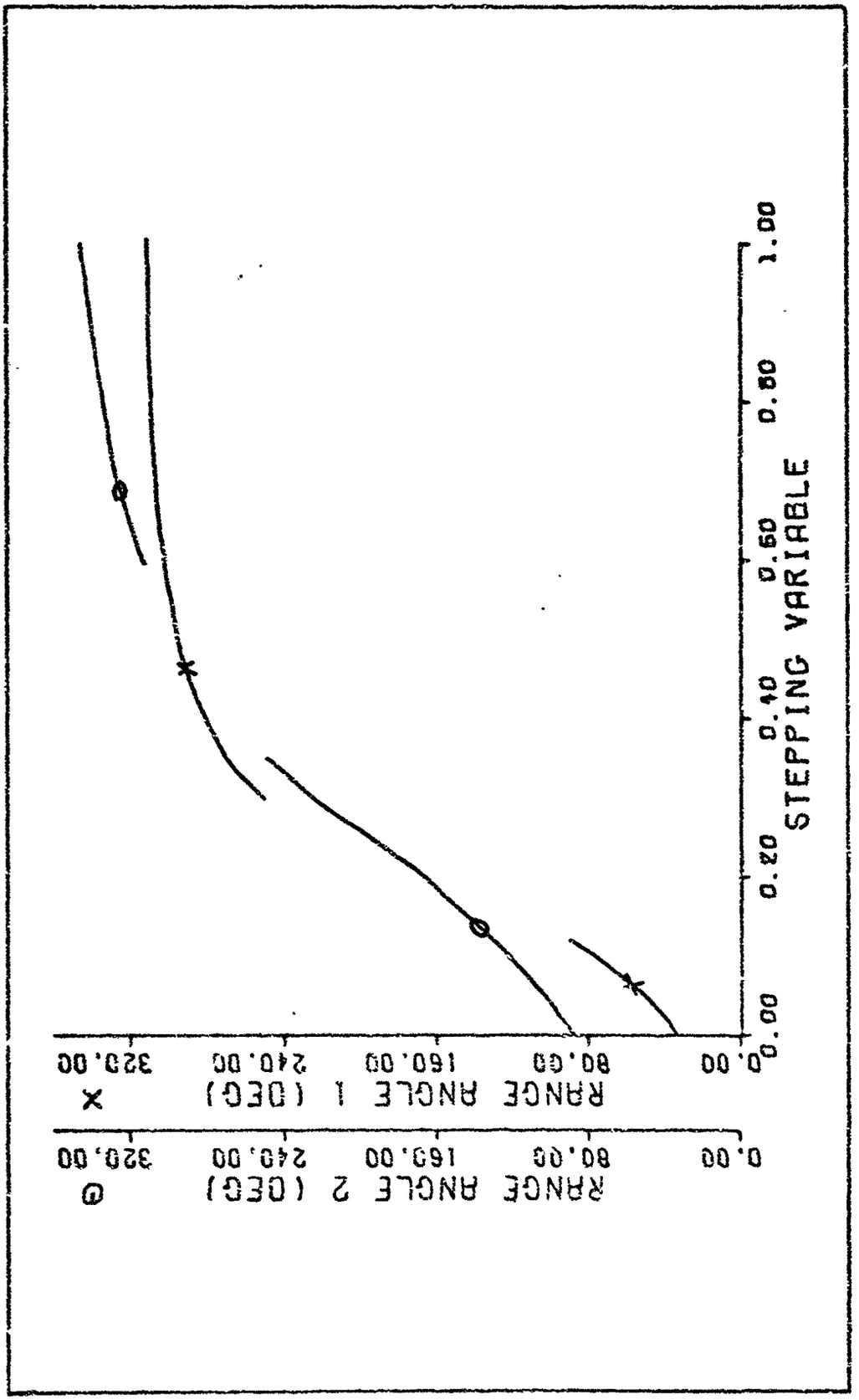

Fig. 4. Ballistic Phase Range Division

the values of Q and δ which exist at the beginning of the terminal phase due to free flight symmetry.

The range contributed by the pull up phase and the skipout phase are determined later from computer data.

Reference Trajectory

The cost function chosen for the optimization method is based on errors between the actual trajectory and a reference trajectory. (The cost function is presented in the next section).

The purpose of this section is to present the equations used to obtain a reference trajectory for the skipout phase of flight. This reference path is simply defined as the projection, into the atmosphere, of the desired ballistic phase trajectory (see Fig. 5).

To project the ballistic flight, one can use classical, two-body, orbital mechanics (Ref 3) and the fact that the ballistic trajectory forms part of an orbit. First, the values that remain constant for a particular orbit (orbital constants) must be found. The orbital constants are: specific mechanical energy, E^*,

$$E^* = \frac{V^2}{2} - \frac{\mu}{R} \tag{14}$$

specific angular momentum, h^*,

$$h^* = R\ V \cos\delta \tag{15}$$

the eccentricity, e^*,

$$e^* = \sqrt{1 + \frac{2E^*\ h^{*2}}{\mu^2}} \tag{16}$$

and the length of the semi-latus rectum, p^*,

$$p^* = \frac{h^{*2}}{\mu} \tag{17}$$

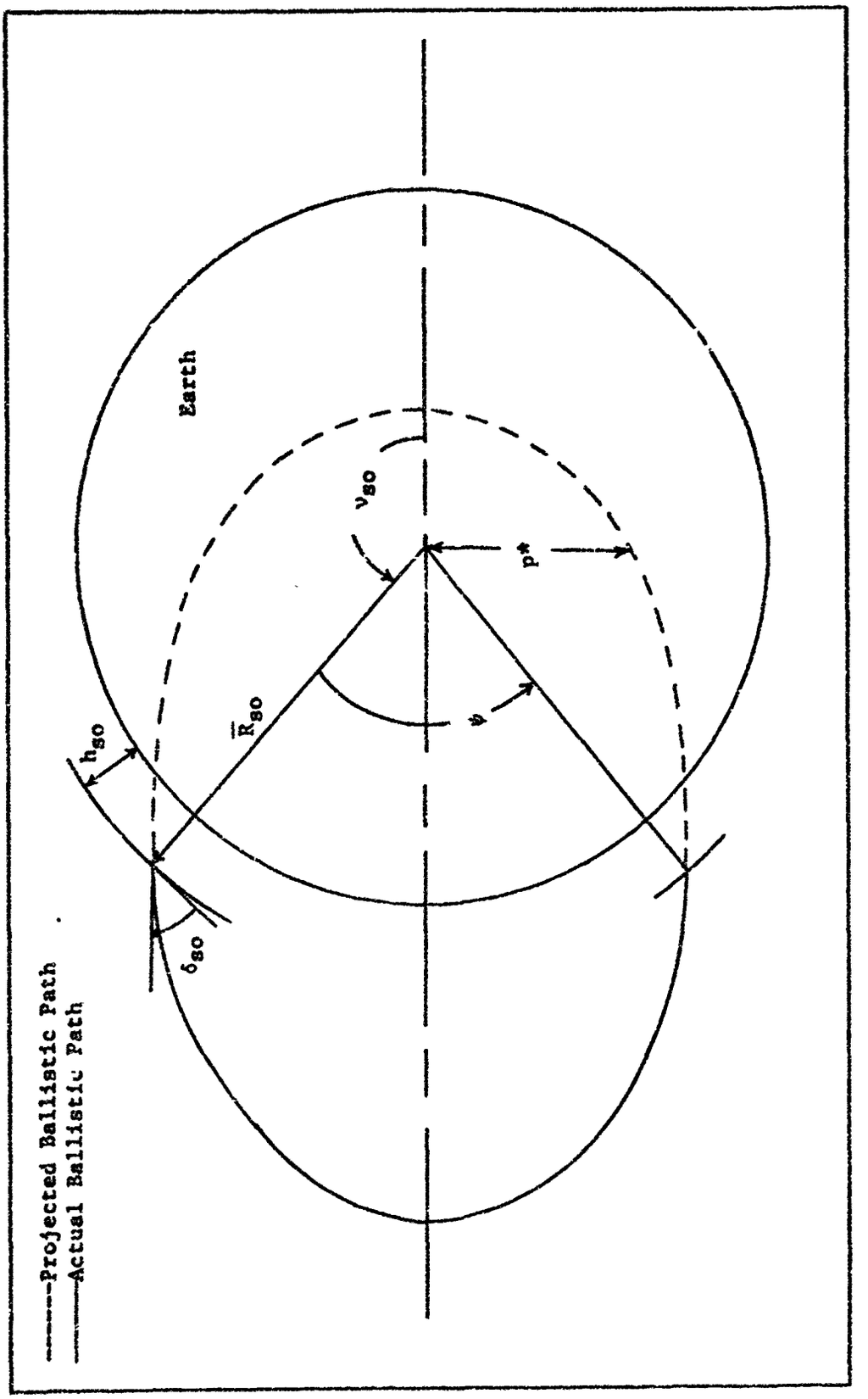

Fig. 5. A Ballistic Trajectory (From Ref 3)

The angle from periapsis to the position radius vector is ν.

$$\nu = \arccos\left[\frac{1}{e^*}\left(\frac{p^*}{R} - 1\right)\right] \tag{18}$$

If the values of V_{so}, R_{so}, δ_{so} are used in equations (14), (15), and (18), the values of E^*, h^*, e^*, p^*, and ν_{so} are then known and can be used as shown next.

Let σ_1 be the total range angle covered by the skipout phase. Let σ_2 be the actual range angle traveled by the RV at an point in the skipout phase (see Fig. 6). Then, as the RV travels along, it has a particular value for R, Q, and δ for each value of σ_2. For the same value of σ_2, a corresponding R, Q, and δ can be found for an imaginary vehicle traveling along the projected ballistic trajectory. The equations used to calculate the states of the imaginary vehicle are given below.

$$\nu_b = \nu_{so} - (\sigma_1 - \sigma_2) \tag{19}$$

$$R_b = \frac{p^*}{1 + e^* \cos \nu_b} \tag{20}$$

$$V_b = \sqrt{2\left(E^* + \frac{\mu}{R_b}\right)} \tag{21}$$

$$Q_b = \frac{V_b^2 R_b}{\mu} \tag{22}$$

$$\delta_b = \arccos\left[\frac{h^*}{R_b V_b}\right] \tag{23}$$

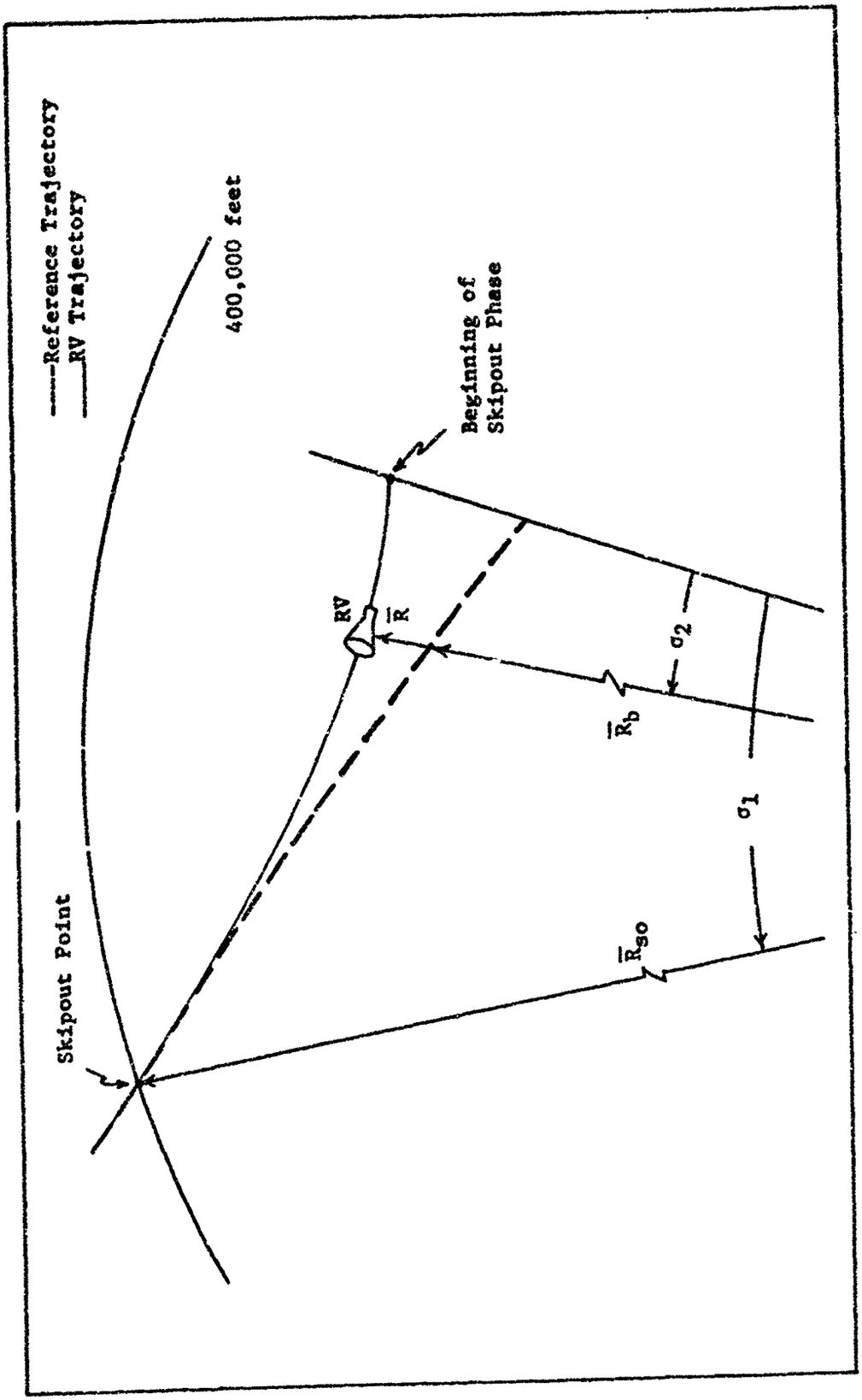

Fig. 6. Actual and Reference Trajectory During Skipout

The differences between the states of the two vehicles (one imaginary) are the errors used in the cost function.

Conjugate Gradient Equations

The equations necessary to apply the conjugate gradient method to the skipout phase are derived in this section, using the theory which is explained in Appendix B.

The cost function to be minimized is

$$J = .5 \int_{s_o}^{s_f} [\bar{e}^T A \bar{e} + (\Delta\alpha) B (\Delta\alpha)] ds + [.5\ \bar{e}^T F\ \bar{e}]_{s=s_f} \tag{24}$$

The term added to the integral is a penalty function on the terminal conditions. The symbol $\Delta\alpha$ is the change in control, and the vector $\bar{e}$ contains the errors between the states of the actual and the reference trajectory.

$$\bar{e} = \begin{bmatrix} e_h \\ e_Q \\ e_\delta \end{bmatrix} = \begin{bmatrix} x_1(s) - h_b(s) \\ x_2(s) - Q_b(s) \\ x_3(s) - \delta_b(s) \end{bmatrix} \tag{25}$$

The weighting matrices are chosen to be

$$A = \begin{bmatrix} A_1 & 0 & 0 \\ 0 & A_2 & 0 \\ 0 & 0 & A_3 \end{bmatrix} \tag{26}$$

$$B = \text{scalar} \tag{27}$$

$$F = \begin{bmatrix} F_1 & 0 & 0 \\ 0 & F_2 & 0 \\ 0 & 0 & F_3 \end{bmatrix} \tag{28}$$

Thus, the cost can be written as

$$\begin{aligned} \text{minimize } J = .5 \int_{s_o}^{s_f} (e_h^2 A_1 + e_Q^2 A_2 + e_\delta^2 A_3 + (\Delta\alpha)^2 B) ds \\ + .5(e_h^2 F_1 + e_Q^2 F_2 + e_\delta^2 F_3)_{s=s_f} \end{aligned} \tag{29}$$

To convert to a Meyer formulation, the integrand of the integral portion of J is made into a state and its differential equation is

$$\frac{dx_4}{ds} = .5(e_h^2 A_1 + e_Q^2 A_2 + e_\delta^2 A_3 + (\Delta\alpha)^2 B) \tag{30}$$

The other states are repeated here for reference.

$$\frac{dx_1}{ds} = -\frac{R}{R_e} \tan\delta \tag{6}$$

$$\frac{dx_2}{ds} = (\tan\delta\ (2-Q) - R\rho \frac{S}{m} \sec\delta\ Q\ C_D) \frac{1}{R_e} \tag{7}$$

$$\frac{dx_3}{ds} = (\frac{1}{Q} - 1 - R\rho \frac{S}{2m} \sec\delta\ C_L) \frac{1}{R_e} \tag{8}$$

Forming the hamiltonian from equations (75), (30), (6), (7), and (8) yields

$$H = -\lambda_1 \frac{R}{R_e} \tan\delta$$

$$+ \lambda_2(\tan\delta\ (2-Q) - R\rho_o\ e^{-\beta h}\ \frac{S}{m}\ Q\ \sec\delta\ C_D)\ \frac{1}{R_e}$$

$$+ \lambda_3(\ \frac{1}{Q} - 1 - R\rho_o\ e^{-\beta h}\ \frac{S}{2m}\ \sec\delta\ C_L)\ \frac{1}{R_e}$$

$$+ \lambda_4\ .5(e_h^2\ A_1 + e_Q^2\ A_2 + e_\delta^2\ A_3 + (\Delta\alpha)^2\ B) \tag{31}$$

The adjoints, from equations (76) and (31), are

$$\frac{d\lambda_1}{ds} = [\lambda_1\ \tan\delta + \lambda_2\ \rho\ \frac{S}{m}\ Q\ \sec\delta\ C_D(1-R\beta)$$

$$+ \lambda_3\ \rho\ \frac{S}{2m}\ \sec\delta\ C_L(1-R\beta)]\ \frac{1}{R_e} - \lambda_4\ e_h\ A_1 \tag{32}$$

$$\frac{d\lambda_2}{ds} = [\lambda_2(\tan\delta + R\rho\ \frac{S}{m}\ \sec\delta\ C_D) + \lambda_3\ \frac{1}{Q^2}\ ]\ \frac{1}{R_e}$$

$$- \lambda_4\ e_Q\ A_2 \tag{33}$$

$$\frac{d\lambda_3}{ds} = [\lambda_1\ R\ \sec^2\delta - \lambda_2(\sec^2\delta(2-Q) + R\rho\ \frac{S}{m}\ Q\ C_D\ \tan\delta\ \sec\delta)$$

$$+ \lambda_3\ R\rho\ \frac{S}{2m}\ C_L\ \tan\delta\ \sec\delta]\ \frac{1}{R_e} - \lambda_4\ e_\delta\ A_3 \tag{34}$$

$$\frac{d\lambda_4}{ds} = 0 \tag{35}$$

$\Rightarrow\ \lambda_4 = \text{constant}$

The transversality conditions are obtained by using equation (77), where

$$\phi(x(s_f)) = x_4(s_f) + .5(e_h^2\ F_1 + e_Q^2\ F_2 + e_\delta^2\ F_3)_{s=s_f} \tag{36}$$

therefore

$$\lambda_1(s_f) = (e_h F_1)_{s=s_f} \tag{37}$$

$$\lambda_2(s_f) = (e_Q F_2)_{s=s_f} \tag{38}$$

$$\lambda_3(s_f) = (e_\delta F_3)_{s=s_f} \tag{39}$$

$$\lambda_4(s_f) = 1 \tag{40}$$

Equations (35) and (40) imply that $\lambda_4(s_f) \equiv 1$, therefore, no integration of equation (35) is required.

Finally, equations (78) and (31) are used to find an expression for the gradient, which must equal zero for an optimal solution.

$$G(\alpha) = -[8.76\ \lambda_2\ Q \sin\alpha \cos\alpha + 1.82\ \lambda_3(2\cos^2\alpha - \sin^2\alpha)] \cdot [\sec\delta \sin\alpha\ \mathrm{sgn}(\alpha)\ \rho \frac{S}{2m} R] \frac{1}{R_e} + \lambda_4(\Delta\alpha)B \tag{41}$$

The equations derived in this section were used in the conjugate gradient algorithm (Appendix B) to obtain an optimal solution for the skipout phase of flight.

Computer Methods

The necessary computer programs were written in Fortran IV language and were executed on a CDC 6600 computer.

The pull up and skipout phases were programmed separately. For the pull up phase, the states were integrated forward until the flight path angle went to zero degrees. The states at that point were used as the

initial conditions for the skipout phase.

For the skipout phase, the conjugate gradient algorithm shown in Appendix B was used. The state and adjoint equations were integrated using a fixed step, Runge-Kutta method. A fixed number of points were necessary to store the state values, which were subsequently used during reverse integration of the adjoint equations. Good results were obtained using arrays of 801 points each for the states, adjoints, gradient, direction of search, control, and perturbated control (used in the alpha search). The total conjugate gradient program used 42K of core memory.

For a set of skip conditions, the penalty terms were initially set to zero while the integral term of the cost function (see equation (29)) was minimized. Then the penalty terms were applied.

The conjugate gradient algorithm was terminated when the cost did not vary in six significant digits.

IV. Results

The re-entry conditions of Apollo 10 were used as the initial conditions for the pull up phase. A constant angle of attack (control) of 54.74° was applied to drive the flight depression angle to zero. This value of control produces the maximum coefficient of lift (see Appendix C). Consequently, the RV does not penetrate the atmosphere too deeply and the nose heat rate peak tends to be minimized. The pull up phase end conditions are summarized in Table I, where the states are h, Q, and δ. The value for velocity was calculated from Q, and the total nose heat is provided as a check for those interested in physical limitations. The largest deceleration force in the pull up phase was approximately 4 g's, which occurred as the flight path angle went to zero.

The pull up phase final conditions shown in Table I were used as initial conditions for the skipout phase. The skipout phase final conditions were found by using a desired ballistic range and the parametric range selection equations, as explained in Chapter III. To make the values of Q_{so} and δ_{so} come out nice the desired ballistic range was chosen as 16,924 nm or 282.07 deg, therefore, from Figures 4 and 2, 'RANGE ANGLE 1' and 'FLT PATH ANGLE 1' were used. For the above range, the stepping variable is 0.4 which gives skipout conditions of $Q_{so} = 1.1$, $\delta_{so} = -4$ deg, and of course $h_{so} = 400{,}000$ ft.

The conjugate gradient technique was then applied for the selected end conditions, using an initial guess of control of 71° (constant). The usual difficulties were encountered in application of the optimal theory and in finding suitable values for the weighting matrices in the cost function, equation (29). The problem with the matrices was that they were sensitive to the skipout conditions and the skipout range selected.

Table I
Pull up Phase End Conditions

(values rounded)

Variable	Initial Condition	Final Condition	Units
s	0.00	380.00	nm
h	400,000.00	218,259.00	ft
Q	2.00	1.72	-
δ	6.61	-0.00	deg
V	36,309.00	33,871.00	ft/sec
q	0.00	11,178.00	BTU/ft^2

Table II
Cost Function Weighting Values

Variable	Value
A_1	$.1 \times 10^{-10}$
A_2	$.1 \times 10^{1}$
A_3	$.1 \times 10^{3}$
B	$.1 \times 10^{0}$
F_1	$.1 \times 10^{3}$
F_2	$.1 \times 10^{13}$
F_3	$.1 \times 10^{15}$

More specifically, a set of weightings that minimized the cost under one set of terminal conditions, would not work using another set, i.e., the alpha search could find no minimum. The weightings finally selected are shown in Table II, and after a few trial runs, a skipout range of 600 nm was finally used.

Convergence to the skipout conditions required 40 iterations, which took 600 seconds of execution time. The conditions were reached with less than 1% error, which resulted in a ballistic phase range error of approximately +80 nm. The convergence errors are summarized in Table III, and the optimal states are shown converging on the reference trajectories in Figures 7, 8, and 9. The optimal control is presented in Fig. 10.

The maximum deceleration in the skipout phase was 8 g's and the peak heat rate was 385 BTU/ft^2·sec. Both of these occurred when the control went to 90°, which gives maximum drag (see Fig. 10), at the beginning of the trajectory. The total nose heat at the end of the optimal skipout trajectory was approximately 24,400 BTU/ft^2. The skipout phase time of flight was 132 seconds.

The approximate surface range traveled for the entire flight is totaled in Table IV.

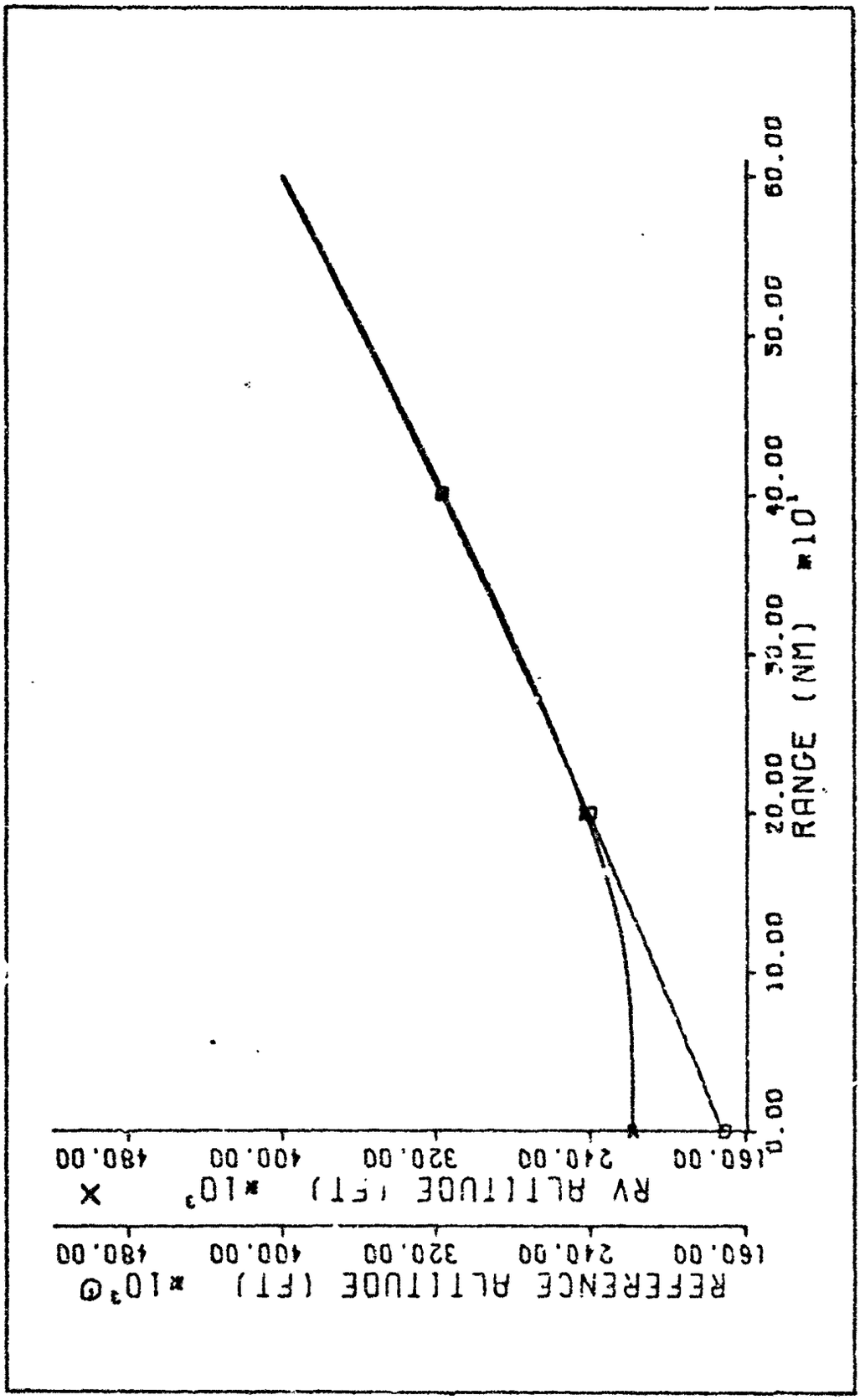

Fig. 7. Optimal Altitude Trajectory

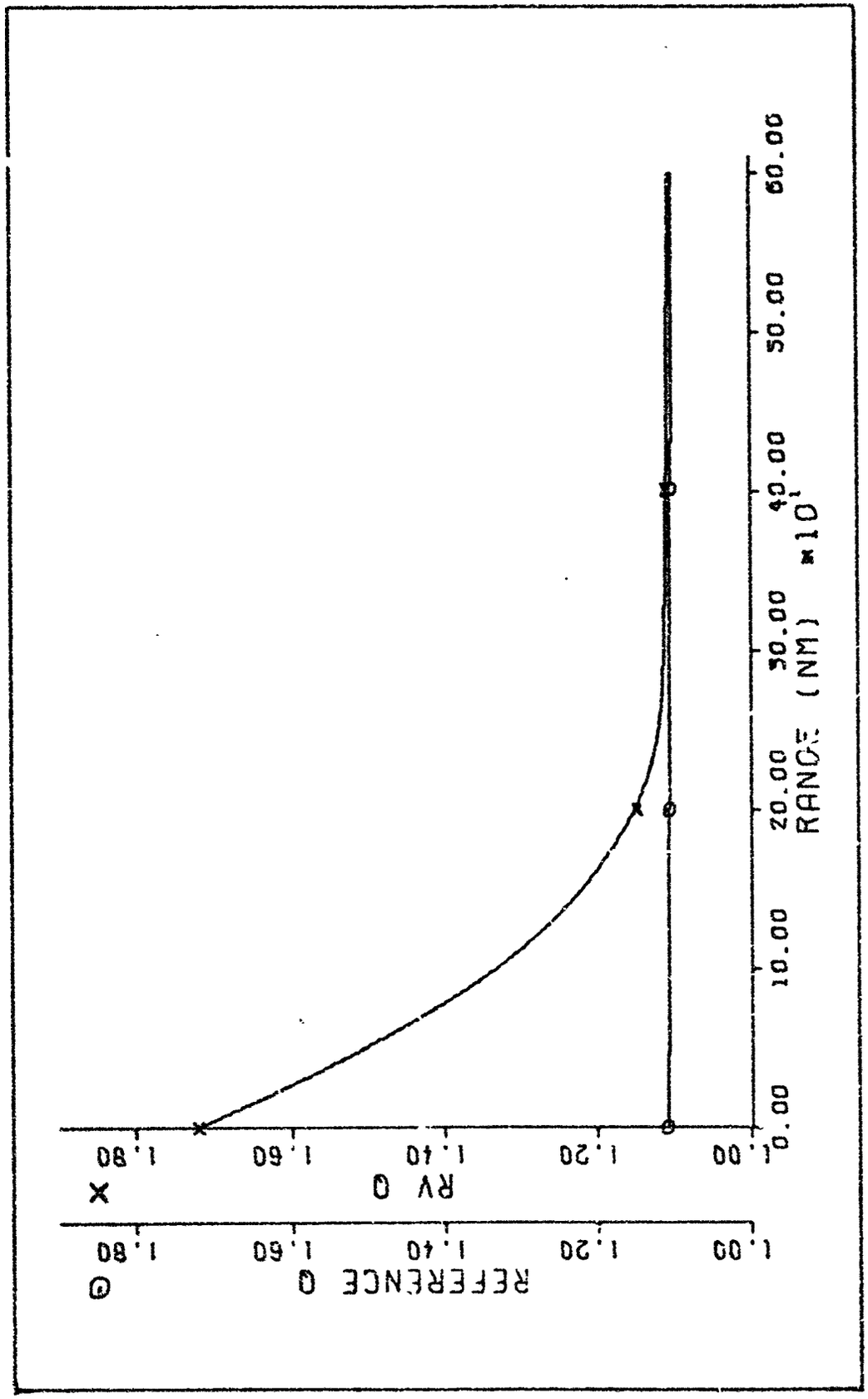

Fig. 8. Optimal Q Trajectory

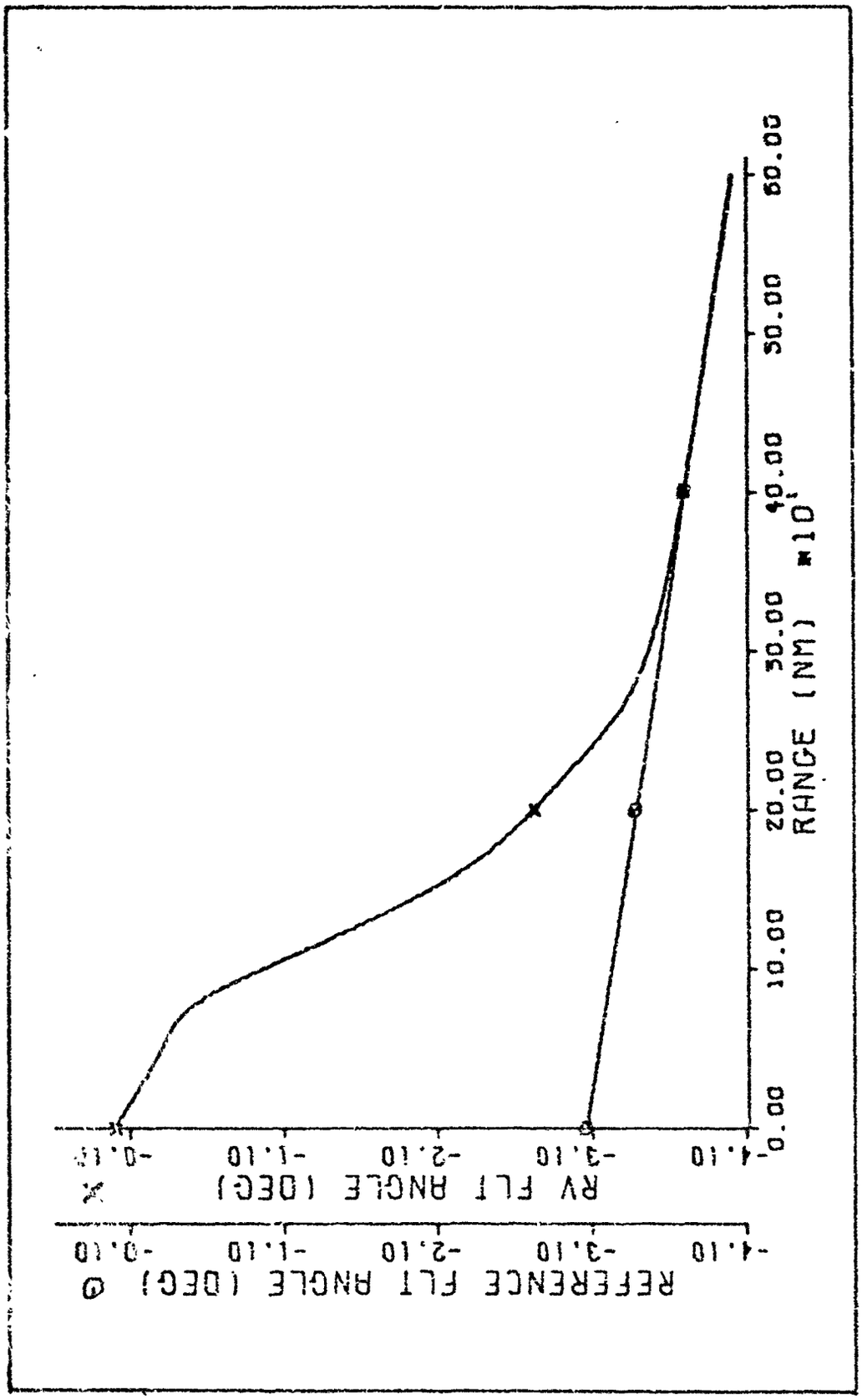

Fig. 9. Optimal Flight Path Angle Trajectory

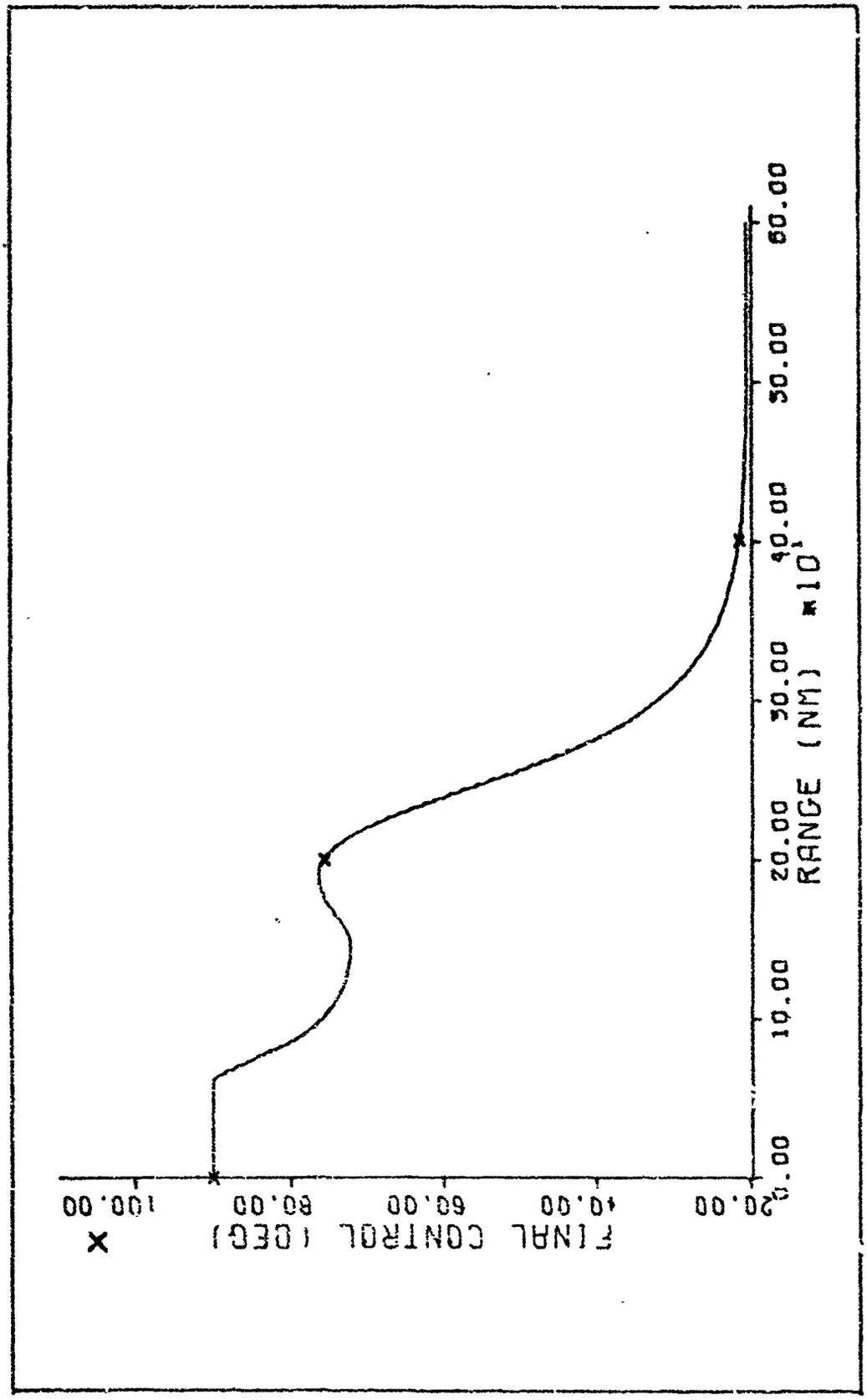

Fig. 10. Optimal Control Trajectory

Table III
Conjugate Gradient Terminal Errors

State	Desired Value	Actual Value	% Error
h	400,000.0	399,763	0.059
Q	1.1	1.10346	0.31
δ	-4.0	-4.03010	0.75

Table IV
Total Surface Range

(values rounded)

	Range (nm)	Range (deg)
Pull up Phase	380	6.4
Skipout Phase	600	10.0
Ballistic Phase	17,000	283.3
Terminal Phase	1,000	16.6
Totals	18,980	316.3

V. Conclusions

A re-entry guidance scheme that utilizes ballistic flight to attain more surface range is feasible, although the deceleration forces and the peak heat rate may be high at the beginning of the skipout phase due to the sudden application of full drag.

The total surface range available depends upon the values of Q_{so} and δ_{so} selected for the ballistic phase and upon the surface range assigned to the other three phases. The minimum and maximum ballistic range is calculated in Chapter III for $0.9 \leq Q_{so} \leq 1.4$ and $2° \leq \delta_{so} \leq 7°$. Using the other ranges listed in Table IV, the total surface range available for re-entry is between 67.5° (4050 nm) and 379° (22,740 nm). The maximum range is greater than one circumference of the Earth. For different boundaries on Q_{so} and δ_{so} in the range selection equations, shorter or longer total distances are possible.

The conjugate gradient technique is suitable for finding an optimal control, but the weighting values in the cost function, equation (29), change as a function of the skipout phase terminal conditions. Consequently, a significant change in terminal conditions requires changes in the weighting values.

However, due to the long execution time involved for convergence (600 seconds), the conjugate gradient method is an unrealistic choice as an onboard, real time controller. A real time controller is needed which is capable of finding the control necessary for the skipout phase. The computation should be performed during pull up and could be based on expected pull up phase terminal conditions. Adjustments would have to be made for any errors between the expected terminal conditions and the actual terminal conditions.

Any further investigations in this area should be made using an optimal scheme that is better suited than the conjugate gradient method, to meet terminal conditions.

Bibliography

1. Graves, Claude A. and Jon C. Harpold. Apollo Experience Report - Mission Planning for Apollo Entry. NASA Technical Note D-6725. Washington: National Aeronautics and Space Administration, March 1972.

2. Bryson, A. E. and W. F. Denham. "A Steepest Ascent Method for Solving Optimum Programming Problems." Journal of Applied Mechanics, VOL 20: 247-255, (June 1962).

3. Bate, Roger R., Donald D. Mueller, and Jerry E. White. Fundamentals of Astrodynamics. New York: Dover Publications, Inc., 1971.

4. Broxmeyer, Charles. Inertial Navigation Systems. New York: McGraw-Hill Book Co., 1964.

5. Lasdon, L. S., S. K. Mitter, and A. D. Waren. "The Conjugate Gradient Method for Optimal Control Problems." IEEE Transactions of Automatic Control, VOL AC-12, NO. 2: 132-138, (April 1967).

Appendix A

Derivation of State Equations

The equations that describe the motion of an unpowered lifting body (re-entry vehicle) in the Earth's atmosphere are derived in this appendix, using the assumptions made in chapter II.

Coordinate System

The geometric relations used are shown in Fig. 11. The coordinate frame E is a locally inertial, Earth centered frame where axis E_1 is aligned with the initial point of atmospheric re-entry.

The coordinate frames, in addition to being right-handed, orthogonal, and cartesian, were chosen such that each vector would be aligne. with a certain axis. The coordinate frames rotate with their respective vectors, therefore, they also serve as a reference for the angle of attack $\alpha(t)$ and the flight depression angle $\delta(t)$.

From Fig. 11 the vectors can be expressed in matrix form as

$$\text{(radius)} \qquad R_M = \begin{bmatrix} R \\ 0 \\ 0 \end{bmatrix} \tag{42}$$

$$\text{(velocity)} \qquad V_N = \begin{bmatrix} 0 \\ V \\ 0 \end{bmatrix} \tag{43}$$

$$\text{(lift)} \qquad L_N = \begin{bmatrix} L \\ 0 \\ 0 \end{bmatrix} \tag{44}$$

$$\text{(drag)} \qquad D_N = \begin{bmatrix} 0 \\ -D \\ 0 \end{bmatrix} \tag{45}$$

$$\text{(gravity)} \qquad g_M = \begin{bmatrix} -\frac{\mu}{R^2} \\ 0 \\ 0 \end{bmatrix} \tag{46}$$

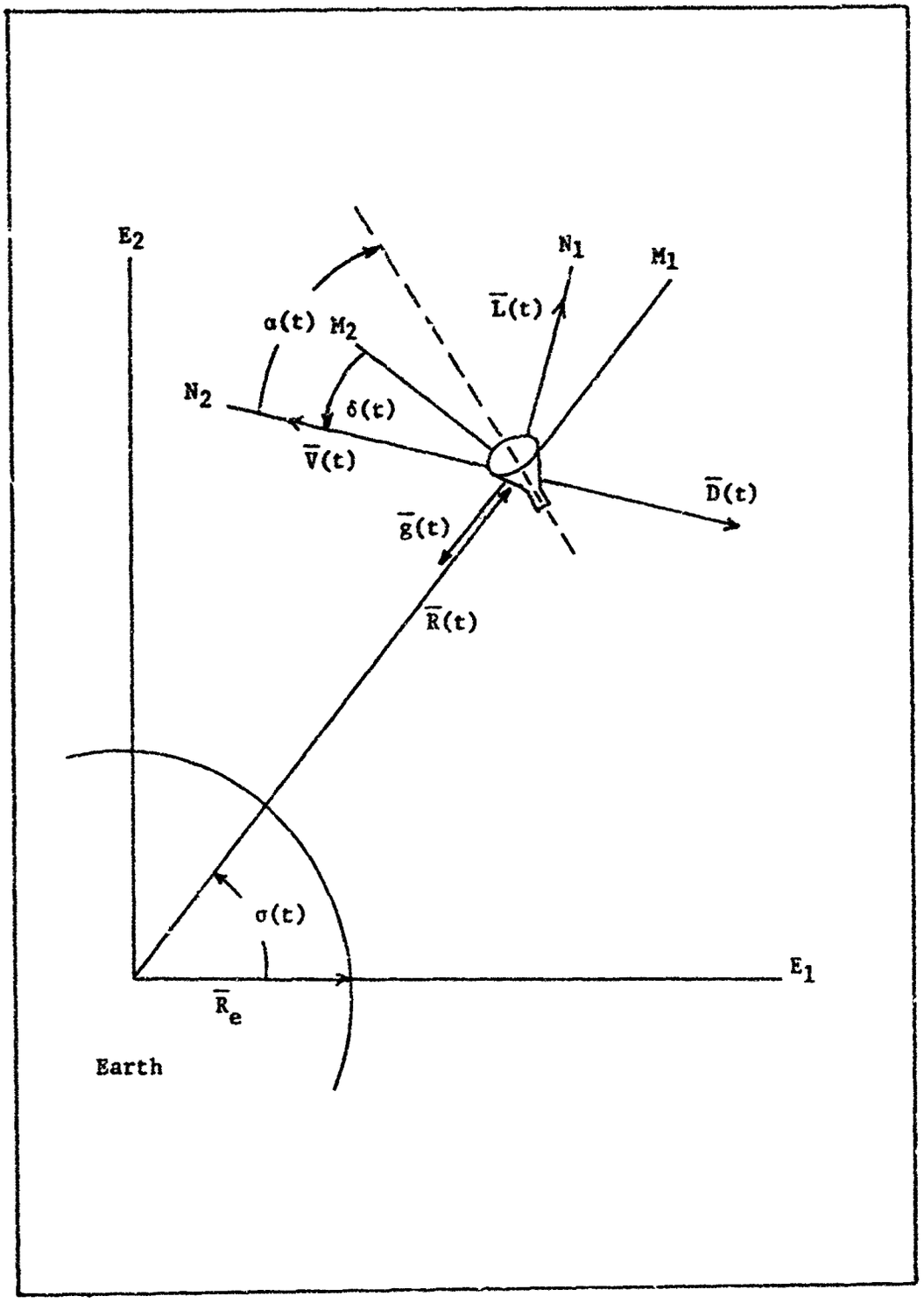

Fig. 11. Geometry of the Problem

where the subscript refers to the coordinate frame in which the vector is measured.

The angular rotation rates are

$$\omega_{EM} = \begin{bmatrix} 0 \\ 0 \\ \frac{d\sigma}{dt} \end{bmatrix} \tag{47}$$

$$\omega_{MN} = \begin{bmatrix} 0 \\ 0 \\ \frac{d\delta}{dt} \end{bmatrix} \tag{48}$$

or, in skew-symmetric form

$$\omega_E^M = \begin{bmatrix} 0 & -\frac{d\sigma}{dt} & 0 \\ \frac{d\sigma}{dt} & 0 & 0 \\ 0 & 0 & 0 \end{bmatrix} \tag{49}$$

$$\omega_M^N = \begin{bmatrix} 0 & -\frac{d\delta}{dt} & 0 \\ \frac{d\delta}{dt} & 0 & 0 \\ 0 & 0 & 0 \end{bmatrix} \tag{50}$$

where the equation ω_{EM} is the angular velocity of the M frame with respect to the E frame.

The coordinate transformations are

$$C_E^M = \begin{bmatrix} \cos\sigma & -\sin\sigma & 0 \\ \sin\sigma & \cos\sigma & 0 \\ 0 & 0 & 0 \end{bmatrix} \tag{51}$$

$$C_M^N \quad \begin{bmatrix} \cos\delta & -\sin\delta & 0 \\ \sin\delta & \cos\delta & 0 \\ 0 & 0 & 1 \end{bmatrix} \tag{52}$$

where transformation is from the frame denoted by the superscript to the frame denoted by the subscript.

Derivation of the Time Derivatives

The next step is to equate velocity (acceleration) components obtained through coordinate transformations, with velocity (acceleration) components obtained by using the theorem of Coriolis (Ref 4: Chap 2). Therefore, the desired equations are

$$V_M = C_M^N V_N \tag{53}$$

$$V_M = \dot{R}_M + \omega_M^E R_M \tag{54}$$

$$a_N = C_N^M g_M + L_N + D_N \tag{55}$$

$$a_N = \dot{V}_N + \omega_N^E V_N \tag{56}$$

Using the appropriate forms of equations (42), (43), (47), and (52) to substitute into the right-hand side of equations (53) and (54), and equating the results, one obtains

$$\begin{bmatrix} -V \sin \delta \\ V \cos \delta \\ 0 \end{bmatrix} = \begin{bmatrix} \dot{R} \\ R\dot{\sigma} \\ 0 \end{bmatrix} \tag{57}$$

From the first row of equation (57)

$$\dot{R} = \frac{dR}{dt} = -V \sin \delta \tag{58}$$

Likewise, the second row yields

$$\dot{\sigma} = \frac{d\delta}{dt} = \frac{V}{R} \cos \delta \tag{59}$$

Following the same procedure for equations (55) and (56), one obtains

$$\begin{bmatrix} 0 \\ \dot{V} \\ 0 \end{bmatrix} = \begin{bmatrix} -\frac{\mu}{R^2}\cos\delta + L + V(\dot{\sigma} + \dot{\delta}) \\ \frac{\mu}{R^2}\sin\delta - D \\ 0 \end{bmatrix} \tag{60}$$

Use of equation (59) and rearrangement of row 1 provides

$$\dot{\delta} = \frac{d\delta}{dt} = \frac{\mu}{VR^2}\cos\delta - \frac{V}{R}\cos\delta - \frac{L}{V} \tag{61}$$

The final equation, which is given in row 2 of equation (60), is

$$\dot{V} = \frac{dV}{dt} = \frac{\mu}{R^2}\sin\delta - D \tag{62}$$

The equations just derived represent the motion of a re-entry vehicle with respect to time. The equations will subsequently be referred to as the state equations or states, and they are summarized below.

$$\frac{dh}{dt} = -V\sin\delta \tag{58}$$

$$\frac{d\sigma}{dt} = \frac{V}{R}\cos\delta \tag{59}$$

$$\frac{dV}{dt} = \frac{\mu}{R^2}\sin\delta - D \tag{62}$$

$$\frac{d\delta}{dt} = \frac{\mu}{VR^2}\cos\delta - \frac{V}{R}\cos\delta - \frac{L}{V} \tag{61}$$

where, in equation (58), it was decided to use altitude rather than radius. Since $R = R_e + h$, the time rate of change is the same for either variable.

Change of Independent Variable

Time is the independent variable in the states above, but in the problem formulation, surface range, s, is of interest. Conversion from

time to range as the independent variable is accomplished using equation (59) and the fact that

$$s = \sigma R_e \tag{63}$$

Also, the range angle, σ, in equation (59) does not appear in any other state equation, so it can be eliminated as a state.

The inverse of equation (59) is

$$\frac{dt}{d\sigma} = \frac{R}{V \cos \delta} \tag{64}$$

or

$$dt = \frac{R}{V \cos \delta} d\sigma \tag{65}$$

The derivative of equation (63) is, after rearrangement

$$d\sigma = \frac{ds}{R_e} \tag{66}$$

Substituting for $d\sigma$, equation (65) becomes

$$dt = \frac{R}{V \cos \delta \, R_e} ds \tag{67}$$

Replacing dt in equations (58), (61), and (62), and after multiplying, the new states become

$$\frac{dh}{ds} = - \frac{R}{R_e} \tan \delta \tag{6 }$$

$$\frac{dV}{ds} = \left(\frac{\mu}{R V} \tan \delta - \frac{D R}{V \cos \delta} \right) \frac{1}{R_e} \tag{68}$$

$$\frac{d\delta}{ds} = \left(\frac{\mu}{V^2 R} - 1 - \frac{L R}{V^2 \cos \delta} \right) \frac{1}{R_e} \tag{69}$$

with surface range as the independent variable. Since the time of flight is not of primary interest here, the equations are now in a more useful

form. Also, the number of equations to be integrated has been reduced from four to three. However, one change remains to be made.

Q as a State

The states are currently written in terms of R, V, and δ, but the charts and equations which cover ballistic theory are written in terms of Q and δ (see Chap III). Consequently, it is advantageous to have Q as a state rather than V. The derivation of dQ/ds follows, starting with the definition of Q.

$$Q = V^2 R/\mu \tag{9}$$

The derivative with respect to range is

$$\frac{dQ}{ds} = \frac{1}{\mu} \left(V^2 \frac{dR}{ds} + 2 R V \frac{dV}{ds} \right) \tag{70}$$

Substituting equations (6) and (68) for the derivatives on the right side, and rearranging, yields the final form.

$$\frac{dQ}{ds} = \left(\tan \delta \, (2-Q) - R\rho \frac{S}{m} \sec \delta \, Q \, C_D \right) \frac{1}{R_e} \tag{7}$$

The value of velocity, if needed, is found from equation (9), i.e.

$$V = \sqrt{Q\mu/R} \tag{71}$$

Equations (68) and (69) must now be rewritten in terms of the new state, Q. The final form of the state equations used for simulation are summarized here and in Chapter II.

$$\frac{dx_1}{ds} = \frac{dh}{ds} = -\frac{R}{R_e} \tan \delta \tag{6}$$

$$\frac{dx_2}{ds} = \frac{dQ}{ds} = \left(\tan \delta \, (2-Q) - R \rho \frac{S}{m} \sec \delta \, Q \, C_D \right) \frac{1}{R_e} \tag{7}$$

$$\frac{dx_3}{ds} = \frac{d\delta}{ds} = \left(\frac{1}{Q} - 1 - R\,\rho\,\frac{S}{2m}\,\sec\,\delta\,C_L \right) \frac{1}{R_e} \qquad (8)$$

Appendix B

Conjugate Gradient Theory

The general theory of the conjugate gradient minimization technique is covered in this appendix. Also, the computational algorithm used to find the optimal control is presented. Much of the material below is taken directly from Ref 5.

General

The conjugate gradient method (Ref 5) is a minimization technique that can be applied to optimal control problems. A solution requires knowledge of the gradient trajectory, its norm, and the actual direction of search. The search direction is found by use of the norm to modify the gradient direction, consequently, each search is in the conjugate direction. Thus, even for a poor initial guess of the optimal control, the method tends to converge.

There are a couple of disadvantages to the conjugate gradient technique. First, the method applies only to unconstrained problems. However, if terminal conditions or inequality constraints are present, penalty functions can be used to convert the problem to an unconstrained form. A second disadvantage is that it is unable to distinguish between a local and a global minimum, which is a fault common to most minimization schemes.

The general problem formulation is for the Meyer form of an optimal control problem.

$$\text{minimize } J = \phi(\bar{x}(t_f)) \tag{72}$$

$$\text{subject to } \dot{\bar{x}} = \bar{f}(\bar{x},\bar{u},t) \tag{73}$$

$$\bar{x}(t_o) = \text{constant} \tag{74}$$

where $\bar{x}$ is an n-order state vector, $\bar{u}$ is an m-order control vector, and the initial time t_o and the final time t_f are fixed. Subsequent discussion of $\bar{u}$ will consider only m=1.

The Hamiltonian is

$$H = \sum_{i=1}^{n} \lambda_i f_i \tag{75}$$

where the adjoints are

$$\frac{d\lambda_i}{dt} = - \sum_{j=1}^{n} \lambda_j \frac{\partial f_j}{\partial x_i}, \quad i=1,\ldots,n \tag{76}$$

and

$$\lambda_i(t_f) = \frac{\partial \phi}{\partial x_i}\Big|_{t=t_f}, \quad i=1,\ldots,n \tag{77}$$

The gradient is

$$G(u) = \frac{\partial H}{\partial u} \tag{78}$$

A necessary condition for $\bar{x}$ to be an optimal state trajectory is that the gradient equal zero for the optimal control trajectory. Thus, the optimal control minimizes the Hamiltonian. The algorithm described in the next section is an iterative process used to find that control.

Computational Algorithm

After the Hamiltonian, adjoint, and gradient equations have been derived, the optimal control can be found by following the steps listed below. The subscript i refers to the previous value.

1. Select an arbitrary control trajectory (often chosen as a constant) and use it to integrate the state equations forward. Proceed to step (3).

2. Perform an alpha search. This consists of finding a distance

α', such that

$$J(u_{i+1}) = J(u_i + \alpha' s_i') \tag{79}$$

is minimized. This requires forward integration of the states until equation (79) is satisfied.

3. Integrate the adjoint equations backwards as a function of the final state values.

4. Compute the gradient from the states and adjoints.

5. Calculate a new direction of search s' according to

$$s_{i+1}' = -G_{i+1} + \beta_{i+1}' s_i' \tag{80}$$

with

$$\beta_{i+1}' = ||G_{i+1}^2||/||G_i^2|| \tag{81}$$

where the norm is defined as

$$||G_i^2|| = \int_{t_o}^{t_f} G_i^2 \, dt \tag{82}$$

For the initial iteration, $s_1' = - G_1$

6. Repeat steps (2-5) until the value of cost in step (2) changes less than some tolerance. The current value of control in step (2) will be the optimal control.

Appendix C

Plot of Lift Coefficient versus Angle of Attack

This appendix contains a plot of the coefficient of lift versus the angle of attack (see Fig. 12). The equation for the coefficient of lift is found in Chapter II and is repeated here.

$$C_L = 1.82 \sin\alpha \cos\alpha \, |\sin\alpha|$$

The maximum value of C_L occurs at an angle of 54.74 degrees.

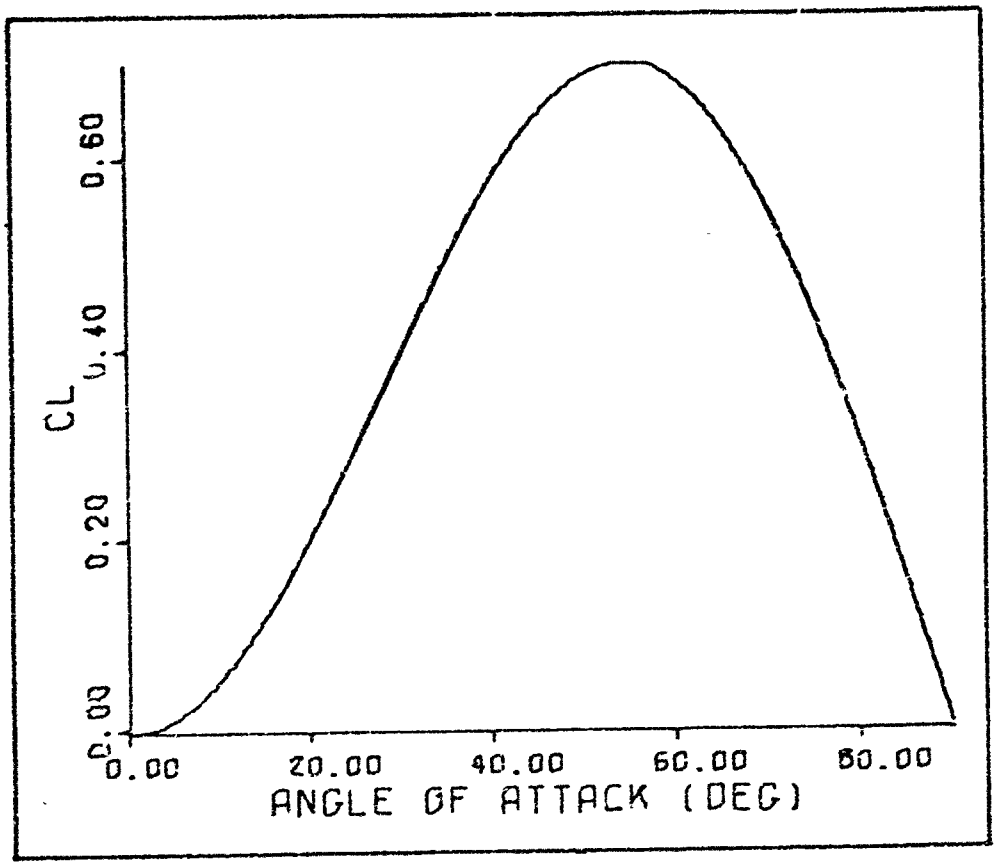

Fig. 12. Lift Coefficient vs. Angle of Attack

Vita

Melvin L. Nagel was born on 20 October 1944 in Hermann, Missouri. He graduated from Hermann High School in June 1962 and immediately enlisted in the Air Force. His first assignment after completing technical school was to a Titan II missile unit, SAC, at McConnell AFB, Kansas. There, for six years, Airman Nagel was a Missile Facilities Technician on a Combat Ready Instructor Crew. While stationed at McConnell, he began taking night classes at Wichita State University. After accruing enough semester hours, he was sent, under the Airmans Education and Commissioning Program, to Oklahoma State University. There he received a Bachelor of Science Degree in Electrical Engineering in 1971. After attending OTS, he was commissioned a Second Lieutenant in September 1971. Lt Nagel was then transferred to AFIT where he received his Master of Science Degree in Electrical Engineering in June 1973.

Permanent Address: 223 West Seventh Street
Hermann, Missouri 65041

This thesis was typed by Miss Sherry L. Willman.